

Atomic Collapse in Disordered Graphene Quantum Dots

Mustafa Polat¹ and A. D. Güçlü¹

¹*Izmir Institute of Technology, Department of Physics, 35430 Urla, Izmir, Turkey**

(Dated: March 20, 2022)

In this paper, we numerically study a Coulomb impurity problem for interacting Dirac fermions restricted in disordered graphene quantum dots. In the presence of randomly distributed lattice defects and spatial potential fluctuations, the response of the critical coupling constant for atomic collapse is mainly investigated by local density of states calculations. As a result of random disorders, up to thirty-four percent increase in the critical threshold is reported. This numerical result may explain why the Coulomb impurities remain subcritical in experiments, even if they are supercritical in theory.

Quantum electrodynamics predicts that the $1S_{1/2}$ state is only stable up to a critical nuclear charge $Z_c \sim 172$; otherwise, formerly bound state becomes a resonant state [1]. In spite of its long-standing history [2], collapse of the vacuum is far from being proven in experiments performed with real atoms [3]. However, graphene reduces the critical threshold to $Z_c \gtrsim 1$ through a larger fine structure constant $\alpha = 2.2/\kappa$ [4, 5], where κ is the dielectric constant. Therefore, the idea of creating an artificial supercritical atom with a smaller critical valence charge has received considerable experimental attention [6–10]. In the condensed matter analogue, Dirac fermions form the vacuum itself, and the Coulomb impurity acts as a nucleus within the vacuum [11]. The main physics behind the model is to calculate a critical coupling constant $\beta_c = Z_c \alpha$ above which is referred to as the supercritical regime [12]. This critical value is estimated to be $\beta_c = 0.5$ for a vacuum consisting of non-interacting massless Dirac fermions [4, 5], and β_c remains the same when these fermions are confined in smaller-sized graphene quantum dots (GQDs) [13, 14]. A further extension of the problem takes electron interactions into account [15, 16] for which the critical coupling constant is renormalized to $\beta_c = 0.6$ due to off-site Coulomb repulsion among Dirac particles [14]. On the exceeding values of the coupling strength β , the lowest energy electron state is bound to the impurity as the $1S_{1/2}$ state [5]. Similarly, the Coulomb impurity can host an infinite number of supercritical states for larger values of β [4]. These states can be measured as spatially extended resonances in a table-top experimental setup [6–8], but the theoretically assumed perfect vacuum order may be broken in practice [17, 18].

Atomic scale defects [19, 20] and the intercalation of hydrogen atoms [21–23] may arise during the growth process, and these defects lead to an imperfect honeycomb lattice [24, 25]. Furthermore, such a deformed vacuum can fluctuate in response to spatial charge inhomogeneities caused by substrate [26, 27]. However, effects of these imperfections on the critical threshold are not yet opened for discussion. In this manner, the hexagonal GQDs with armchair edges [28] could provide a practical playground to find out ambiguous consequences

of these distortions beyond conventional perspective of the theory. As evidenced by transmission coefficients of the $1S_{1/2}$ state [14], these special GQDs [28, 29] serve as a bridge between the finite-sized samples and bulk graphene by rendering the size of the vacuum negligible for the Coulomb impurity problem. This remarkable result could help in finding solutions to such complex problems via exact diagonalization of Hamiltonian, even in the case of interacting fermions.

In this letter, the critical threshold is studied by placing the Coulomb impurity at the center of disordered hexagonal GQDs. Deviations from the perfection in the vacuum are deliberately created by: (i) randomly distributed point vacancies with different concentrations and (ii) electron-hole puddles induced by Gaussian impurities. In short, a strong dependence of the critical threshold on these disorders is reported, and up to thirty-four percent increase in the critical coupling constant is achieved.

Extended mean-field Hubbard model is employed to study the π_z dynamics, and the Hamiltonian reads

$$H_{MFH} = t \sum_{\langle ij \rangle \sigma} (c_{i\sigma}^\dagger c_{j\sigma} + \text{H.c.}) + U \sum_{i\sigma} \left(\langle n_{i\bar{\sigma}} \rangle - \frac{1}{2} \right) n_{i\sigma} + \sum_{ij} V_{ij} (\langle n_j \rangle - 1) n_i - \hbar v_F \beta \sum_{i\sigma} \frac{c_{i\sigma}^\dagger c_{i\sigma}}{r_i}, \quad (1)$$

where the first term describes the tight-binding Hamiltonian with a hopping amplitude of $t = -2.8$ eV. The operator $c_{i\sigma}^\dagger$ ($c_{i\sigma}$) creates (annihilates) an electron with spin σ at the lattice site i . $U = 16.52/\kappa$ eV is the onsite Coulomb repulsion [29], where $\kappa = 6$ corresponds to the interband polarization [30]. $\langle n_{i\sigma} \rangle$ is the spin-dependent expectation value of electron densities, and $n_{i\sigma}$ is the spin-dependent number operator. Third term V_{ij} is associated with the off-site Coulomb repulsion which is set to be $8.64/\kappa$ eV, $5.33/\kappa$ eV, and $1/\kappa d_{ij}$ eV for the nearest-neighbors, next-nearest-neighbors, and the remote atomic sites, respectively [29, 31]. The last term represents the Coulomb impurity placed at the origin of coordinate system, where r_i is the distance between the impurity and the site i . $v_F \approx 10^6$ m/s is the Fermi velocity.

Atomic vacancies with concentrations of 0.1%, 0.5%, 1%, and 2% are created by randomly and equally removing the two sublattices, A (50%) and B (50%), of the honeycomb lattice [32]. For only 1% concentration of carbon vacancies, the electron-hole puddles are created by the superposition of contributions of randomly distributed Gaussian impurities [33] with a total number of $N_{imp} = 16$. Gaussian potential at a position \mathbf{r}_n can be written as follows: $V_i = \sum_{n=1}^{N_{imp}} \Delta_n \exp \left[-|\mathbf{r}_i - \mathbf{r}_n|^2 / (2\xi^2) \right]$, where Δ is the impurity strength, and the impurity correlation length is taken to be $\xi = 10a$ [34]. Half of these impurities are chosen as positive and the other half as negative with the help of Δ and which randomly fluctuates within three different intervals. The results for each of the above configurations are extracted from averaging over ten different samples to increase consistency.

Local density of states (LDOS) [4] is experimentally accessible through a scanning tunneling microscope (STM) [7] and is calculated by $N(E, r) = \sum_i |\Psi_i(r)|^2 \delta(E - E_i)$, where $\Psi(r)$ is the normalized wave function. The energy E is equivalent to applied bias voltage in STM measurements. Since all calculations are performed for a fixed number of electrons, the Fermi level (FL) moves down starting from the energy origin as β is increased [13, 14].

It can be useful to discuss the effect of the vacuum size from a different perspective before proceeding to the disordered cases. The pristine hexagonal GQDs that differ in size are created, and discrete energy levels of them are summed at the impurity site. Although such a sum corresponding to a family of quasi-bound states (QBS) [5] is not necessary for the perfect vacuums [4], it will provide a considerable advantage in the following sections. All supercritical states are sequentially arranged within this family, and which contains the $1S_{1/2}$ state as the first component. Atomic collapse occurs when this sharp peak in the electronic LDOS crosses just below the Dirac point (DP) [7]. Since the electron states of the GQDs become resonances at the negative energies [13, 14], the energy origin is assumed to be the DP in our numerical calculations [8]. To avoid too cumbersome notation, the critical coupling constant of the families of QBS is represented by $\tilde{\beta}_c$, and only the response of the spin-up Dirac fermions is studied at the impurity site due to the presence of a spin-independent central potential. The spin-up QBS families are shown in Fig. 1(a) for the perfect lattices consisting of 2814, 5514, and 10 806 carbon atoms. All families are pinned at the DP for $\tilde{\beta}_c = 1.0$, and which guarantees the size independence of the problem. The critical bare valence charge is calculated to be $\tilde{Z}_c \approx 2.73$ by taking $\kappa = 6$. As a comparison, the critical coupling constant equals $\beta_c = 0.6$ for only the $1S_{1/2}$ state [14], and Z_c is larger than a unit charge for the interacting fermions [14, 16].

When point defects are randomly distributed, vacancy-induced states appear in the energy spectrum [35]. Since these defect states are localized around the FL

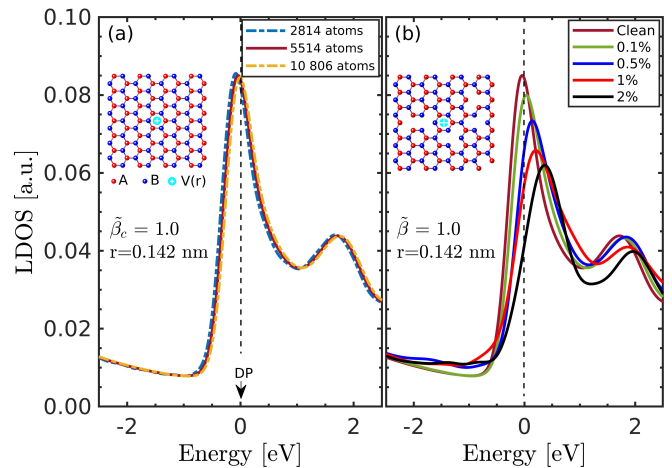


FIG. 1: Local density of states (LDOS) spectra at the impurity site for the numbers of 2814, 5514, and 10 806 atoms in (a). The inset illustrates a zoomed portion of the perfect lattice with a central Coulomb impurity. (b) clearly shows the response of the same spectra in the presence of finite defect densities, and the problem is shown in the inset as a sketch.

[14, 32, 35, 36], they will follow the FL when $\tilde{\beta}$ is turned on [8]. Consequently, the existence of the localized states does not affect the discussion about the DP, and which is again at the energy origin in the presence of the Coulomb impurity. As for the spin symmetry, it is naturally broken in the disordered lattices [32]. However, similar to the clean case, there is no significant difference between the spin-up and spin-down families near $\tilde{\beta}_c$ for a 50% (A) - 50% (B) distribution. These characteristic of the spin components facilitates the access to the spin-up QBS families at the DP for a proper comparison with the clean case. In this manner, we have randomly distributed lattice defects with concentrations of 0.1%, 0.5%, 1%, and 2% over the GQD lattice consisting of 5514 atoms in the pristine case. As is clear from Fig. 1(b), all spin-up QBS families at the impurity site retreat from the DP depending on the concentration of these defects. It points out that $\tilde{\beta} = 1.0$ is no longer a critical coupling constant, and which is the first sign of the effect of lattice imperfections for the atomic collapse states.

These families transit from above to the edge of the DP at different $\tilde{\beta}_c$ which is evident in Fig. 2(a)-(d). The critical coupling constant gradually increases in proportion to the defect densities and reaches $\tilde{\beta}_c = 1.27$ in the presence of 2% defect density; see Fig. 2(d). Actually, these defects are ubiquitous in the crystal structure [24]. For example, the Raman spectrum has ~ 0.5 Gto2D intensity ratio for the high-quality graphene monolayer grown by chemical vapor deposition (CVD) [37], and this ratio indicates that there is a finite defect density in graphene. As is clear from our numerical results, these structural peculiarities can cause an increase in the critical threshold. On the other hand, the shapes of all QBS families

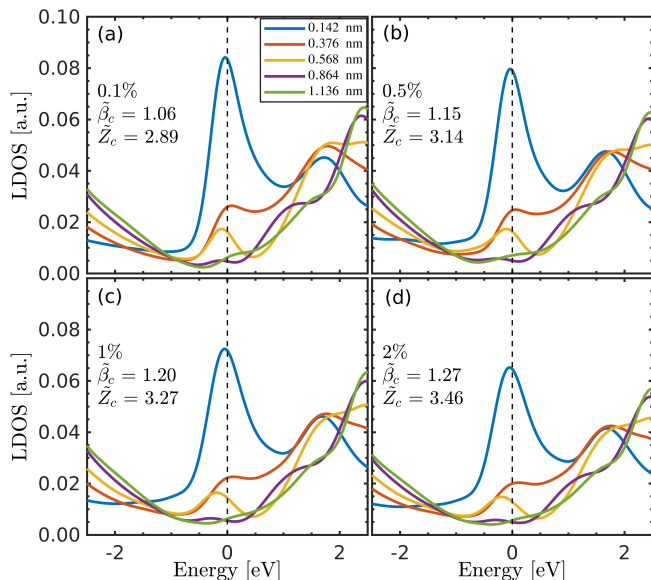


FIG. 2: Defect-induced increase in the critical coupling constant $\tilde{\beta}_c$ for the concentrations of 0.1% in (a), 0.5% in (b), 1% in (c), and 2% in (d). The different colored lines represent the corresponding distances from the impurity.

are the same as of the clean case, especially in the vicinity of the impurity. It can be inferred that atomic collapse is similarly observed in the imperfect lattices, but the supercritical regime can be reached through an impurity with a higher valance charge as can be seen in Fig. 2(a)-(d).

In the case of lattice imperfections, the lowest energy states in the electron channel are the defect states. Therefore, it is obvious that the first responders to the increase of $\tilde{\beta}$ are these unoccupied vacancy-induced states. To elucidate their responses, we study total electron probability density of the spin-up defect states at different $\tilde{\beta}$ for a representative sample with a 1% vacancy concentration. Fig. 3(a)-(d) clearly shows that the $1S_{1/2}$ state emerges from these localized states. There is no explicit crossing from the higher valance states in the energy spectrum revealing that a sum of only empty states creates the lowest supercritical state. Indeed, all defect states extend over many lattice sites starting from the center of vacancies. In Ref. [8], for example, their spatial extensions are measured to be 2 nm. The spatial extensions of such states lead to the formation of the $1S_{1/2}$ state, whereas the strongly localized parts of them preserve the characteristic triangular shape of the mono-vacancies, demonstrating a striking stability against the Coulomb impurity as explicitly seen in Fig. 3(a)-(d). It is clear that more valance charge is required to bound these localized states to the impurity as compared to the lowest unoccupied state of a pristine QD. It explains the increase in the critical threshold from the beginning.

Prior to the collapse experiments [6–9], monolayer

graphene is grown by CVD and then is transferred onto a BN flake placed on a SiO_2/Si substrate. To model the spatial potential fluctuations caused by such a substrate, we randomly distributed Gaussian impurities for the set of vacuum disordered by 1% concentration of carbon vacancies. The averaged potential landscapes of $|\Delta| < 0.3t$ and $|\Delta| < 0.5t$ are shown in Fig. 4(a) and Fig. 4(b), respectively. The resulting electron-hole puddles are only studied for the spin-up fermions, since there will be no difference between the spin components in the presence of spin-independent Gaussian impurities. In particular, the electron puddles (red) appear in the positive potential regions, whereas the hole puddles (blue) manifest themselves in the negative potential regions. The averaged spatial distribution of these charge puddles can be seen in Fig. 4(c) for $|\Delta| < 0.3t$ and Fig. 4(d) for $|\Delta| < 0.5t$. As $\tilde{\beta}$ is turned on, the charge inhomogeneities rearrange themselves under the effect of the Coulomb potential. For $\tilde{\beta} = 1.2$, the electron-hole puddles of $|\Delta| < 0.3t$ and those of $|\Delta| < 0.5t$ are mapped in Fig. 4(e) and Fig. 4(f), respectively. Even if there is no significant change in the positions of the hole puddles formed at the distances away from the center, those close to the center leave their positions and are centered around the stronger Coulomb impurity. As will be seen in the next section, such a reformation has a significant effect on the critical threshold.

LDOS spectra in Fig. 5(a)-(c) are calculated for the spin-up QBS family starting from the impurity site. When the positive and negative Gaussian impurities are

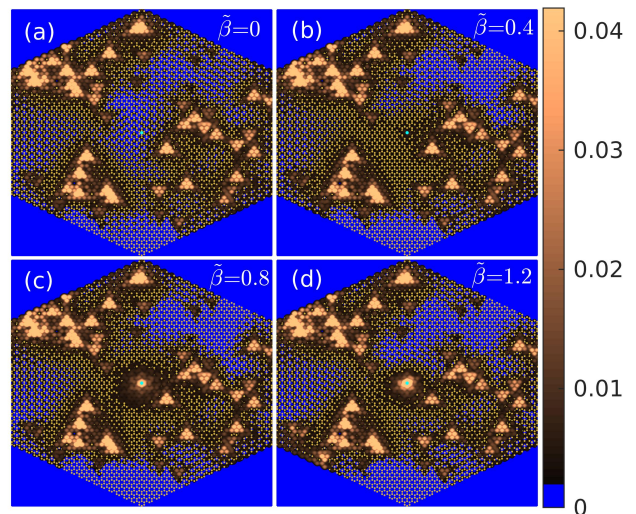


FIG. 3: Response of empty spin-up defect states to the Coulomb field for a representative sample. Their spatial distributions are shown in (a)-(d) for $\tilde{\beta} = 0, 0.4, 0.8$, and 1.2 , respectively. As is clear from (c) and (d), the $1S_{1/2}$ state is formed at the center of QD marked by green dots.

distributed evenly, the total DOS of the spin-up fermions at $\tilde{\beta} = 0$ clearly reveals that the FL is again around the energy origin for these configurations; see the inset in Fig. 5(c). There is no significant shift in the minimum energy point at the beginning allowing us to take the energy origin as the DP for larger values of $\tilde{\beta}$. Similar to the previous cases, whenever the sharp peak enters the negative energy spectrum, then atomic collapse has occurred. As a result, the addition of Gaussian impurities causes to an increase in the critical threshold from $\tilde{\beta}_c = 1.20$ [Fig. 2(c)] up to $\tilde{\beta}_c = 1.34$ [Fig. 5(c)], and the critical valance charge is found to be as high as $\tilde{Z}_c = 3.65$. It can be noted that the increments in the critical threshold are independent of the sign of the substrate-induced potential where the Coulomb impurity is placed, and such increments are directly proportional to the strength of Gaussian impurities.

In bulk graphene, a series of LDOS measurements performed by a STM reveals that a cluster, composed of four calcium dimers in the charge state of $+1|e|$, is needed to form an infinite family of QBS at just above the DP [see Fig. 1(D) in Ref. [7]]. Therefore, the critical bare valance charge should be slightly greater than $\tilde{Z}_c \gtrsim 4$ in the experiment. Accordingly, the calculated values of \tilde{Z}_c are approaching to that of the experiment, and adding these experimentally relevant factors to the Coulomb impurity problem opens a new route towards such experi-

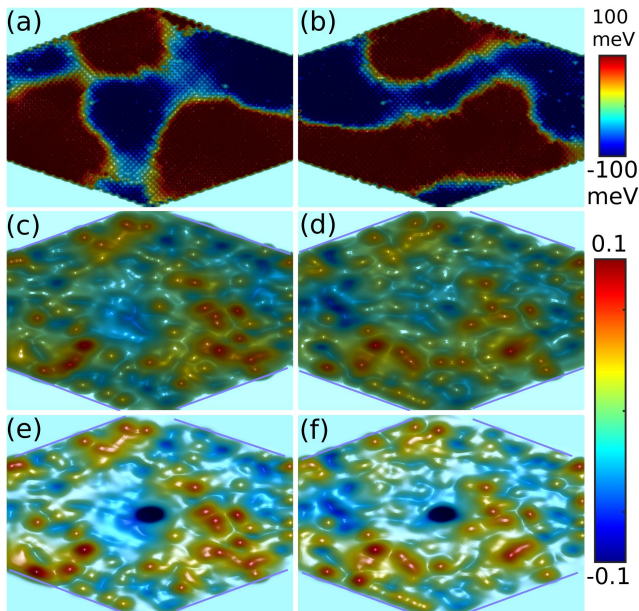


FIG. 4: Averaged potential fluctuations for $|\Delta| < 0.3t$ in (a) and $|\Delta| < 0.5t$ in (b). In the absence of the Coulomb impurity, the spin-up electron-hole puddles are formed in response to $|\Delta| < 0.3t$ in (c) and $|\Delta| < 0.5t$ in (d). For $\tilde{\beta} = 1.2$, the reformation of these charge puddles can be seen in (e) and (f) for $|\Delta| < 0.3t$ and $|\Delta| < 0.5t$, respectively.

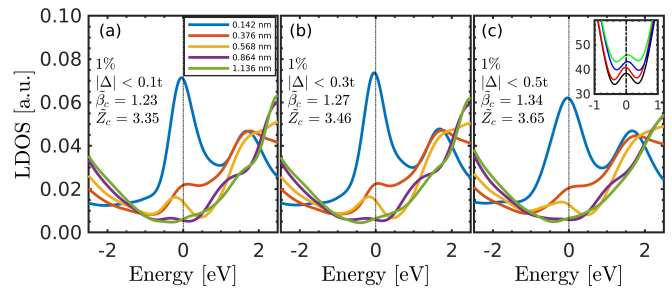


FIG. 5: The effect of spatial charge inhomogeneities on the critical threshold in (a)-(c). The inset in (c) shows averaged total DOS for $\tilde{\beta} = 0$, where black, red, blue, and green lines represent $\Delta = 0$, $|\Delta| < 0.1t$, $|\Delta| < 0.3t$, and $|\Delta| < 0.5t$, respectively. For the sake of simplicity, a space between these lines is intentionally added.

mental results [6, 7]. These findings can be useful in interpreting the experimental results of positively charged Coulomb impurities, even if they exceed the theoretical critical value. Results of this paper can be tested by deliberately hydrogenated [38] and Ar^+ ion bombarded graphene [39]. There should be an increase in the critical threshold due to the partial or complete removal of the π_z states.

This work was supported by The Scientific and Technological Research Council of Turkey (TUBITAK) under 1001 Grant Project No. 116F152.

* Electronic address: mustafapolat@iyte.edu.tr

- [1] J. Reinhardt and W. Greiner, Rep. Prog. Phys. 40, 219 (1977).
- [2] W. Greiner, *Relativistic Quantum Mechanics* (Springer, New York, 2000).
- [3] T. Cowan, H. Backe, M. Begemann, K. Bethge, H. Bockemeyer, H. Folger, J. Greenberg, H. Grein, A. Gruppe, Y. Kido, et al., Phys. Rev. Lett. 54, 1761 (1985).
- [4] A. Shytov, M. Katsnelson, and L. Levitov, Phys. Rev. Lett. 99, 246802 (2007).
- [5] V. M. Pereira, J. Nilsson, and A. C. Neto, Phys. Rev. Lett. 99, 166802 (2007).
- [6] Y. Wang, V. W. Brar, A. V. Shytov, Q. Wu, W. Regan, H.-Z. Tsai, A. Zettl, L. S. Levitov, and M. F. Crommie, Nat. Phys. 8, 653 (2012).
- [7] Y. Wang, D. Wong, A. V. Shytov, V. W. Brar, S. Choi, Q. Wu, H.-Z. Tsai, W. Regan, A. Zettl, R. K. Kawakami, et al., Science 340, 734 (2013).
- [8] J. Mao, Y. Jiang, D. Moldovan, G. Li, K. Watanabe, T. Taniguchi, M. R. Masir, F. M. Peeters, and E. Y. Andrei, Nat. Phys. 12, 545 (2016).
- [9] D. Wong, F. Corsetti, Y. Wang, V. W. Brar, H.-Z. Tsai, Q. Wu, R. K. Kawakami, A. Zettl, A. A. Mostofi, J. Lischner, et al., Phys. Rev. B 95, 205419 (2017).
- [10] J. Lu, H.-Z. Tsai, A. N. Tatan, S. Wickenburg, A. A. Omrani, D. Wong, A. Riss, E. Piatti, K. Watanabe, T. Taniguchi, et al, Nat. Commun. 10, 1 (2019).

- [11] A. C. Neto, F. Guinea, N. M. Peres, K. S. Novoselov, and A. K. Geim, *Rev. Mod. Phys.* 81, 109 (2009).
- [12] V. N. Kotov, B. Uchoa, V. M. Pereira, F. Guinea, and A. C. Neto, *Rev. Mod. Phys.* 84, 1067 (2012).
- [13] R. Van Pottelberge, M. Zarenia, P. Vasilopoulos, and F. Peeters, *Phys. Rev. B* 95, 245410 (2017).
- [14] M. Polat, H. Sevinçli, and A. D. Güçlü, *Phys. Rev. B* 101, 205429 (2020).
- [15] R. R. Biswas, S. Sachdev, and D. T. Son, *Phys. Rev. B* 76, 205122 (2007).
- [16] I. S. Terekhov, A. I. Milstein, V. N. Kotov, and O. P. Sushkov, *Phys. Rev. Lett.* 100, 076803 (2008).
- [17] A. Hashimoto, K. Suenaga, A. Gloter, K. Urita, and S. Iijima, *Nature* 430, 870 (2004).
- [18] J. Martin, N. Akerman, G. Ulbricht, T. Lohmann, J. v. Smet, K. Von Klitzing, and A. Yacoby, *Nat. Phys.* 4, 144 (2008).
- [19] J. C. Meyer, C. Kisielowski, R. Erni, M. D. Rossell, M. Crommie, and A. Zettl, *Nano Lett.* 8, 3582 (2008).
- [20] F. Banhart, J. Kotakoski, and A. V. Krasheninnikov, *ACS Nano* 5, 26 (2011).
- [21] K. M. McCreary, A. G. Swartz, W. Han, J. Fabian, and R. K. Kawakami, *Phys. Rev. Lett.* 109, 186604 (2012).
- [22] W.-X. Wang, Y.-W. Wei, S.-Y. Li, X. Li, X. Wu, J. Feng, and L. He, *Phys. Rev. B* 97, 085407 (2018).
- [23] K. E. Çakmak, A. Altıntaş, and A. D. Güçlü, *Phys. Rev. B* 98, 115428 (2018).
- [24] A. Eckmann, A. Felten, A. Mishchenko, L. Britnell, R. Krupke, K. S. Novoselov, and C. Casiraghi, *Nano Lett.* 12, 3925 (2012).
- [25] S.-Y. Li, Y.-N. Ren, Y.-W. Liu, M.-X. Chen, H. Jiang, and L. He, *2D Mater.* 6, 031005 (2019).
- [26] K. M. Burson, W. G. Cullen, S. Adam, C. R. Dean, K. Watanabe, T. Taniguchi, P. Kim, and M. S. Fuhrer, *Nano Lett.* 13, 3576 (2013).
- [27] H. U. Özdemir, A. Altıntaş, and A. D. Güçlü, *Phys. Rev. B* 93, 014415 (2016).
- [28] A. Güçlü, P. Potasz, and P. Hawrylak, *Phys. Rev. B* 82, 155445 (2010).
- [29] A. D. Güçlü, P. Potasz, M. Korkusinski, and P. Hawrylak, *Graphene Quantum Dots* (Springer, Berlin, 2014).
- [30] T. Ando, *J. Phys. Soc. Jpn.* 75, 074716 (2006).
- [31] P. Potasz, A. Güçlü, and P. Hawrylak, *Phys. Rev. B* 82, 075425 (2010).
- [32] A. Altıntaş and A. D. Güçlü, *Solid State Commun.* 281, 44 (2018).
- [33] J. H. Bardarson, J. Tworzydło, P. Brouwer, and C. Beenakker, *Phys. Rev. Lett.* 99, 106801 (2007).
- [34] Y. Zhang, V. W. Brar, C. Girit, A. Zettl, and M. F. Crommie, *Nat. Phys.* 5, 722 (2009).
- [35] V. M. Pereira, F. Guinea, J. L. Dos Santos, N. Peres, and A. C. Neto, *Phys. Rev. Lett.* 96, 036801 (2006).
- [36] E. B. Kul, M. Polat, and A. D. Güçlü, arXiv:2006.11048 (2020).
- [37] X. Li, W. Cai, J. An, S. Kim, J. Nah, D. Yang, R. Piner, A. Velamakanni, I. Jung, E. Tutuc, et al., *Science* 324, 1312 (2009).
- [38] A. Bostwick, J. L. McChesney, K. V. Emtsev, T. Seyller, K. Horn, S. D. Kevan, and E. Rotenberg, *Phys. Rev. Lett.* 103, 056404 (2009).
- [39] M. M. Lucchese, F. Stavale, E. M. Ferreira, C. Vilani, M. V. d. O. Moutinho, R. B. Capaz, C. A. Achete, and A. Jorio, *Carbon* 48, 1592 (2010).